

---

# Parametric Images of Antibody Pharmacokinetics in Bi213-HuM195 Therapy of Leukemia

Katherine S. Kolbert, Klaus A. Hamacher, Joseph G. Jurcic, David A. Scheinberg, Steven M. Larson, and George Sgouros

*Nuclear Medicine Service, Departments of Radiology and Medical Physics; and Leukemia Service, Department of Medicine, Memorial Sloan-Kettering Cancer Center, New York, New York*

---

Kinetic analysis of gamma camera patient images can provide time-dependent information about antibody behavior. Current region-of-interest-based techniques for the kinetic analysis of these images rely on user selection and drawing of regions to be analyzed. Such analyses do not reveal unexpected kinetic activity outside of the selected regions of interest and do not provide a whole-image assessment regarding the pharmacokinetics of an agent. At Memorial Sloan-Kettering Cancer Center, a method for generating images in which the pixel value represents a kinetic parameter has been developed. This work extends the method into a new application in which whole-body parametric images are used to examine the kinetics of Bi213-HuM195 in patients with leukemia. **Methods:** Bi213-HuM195 is typically administered in multiple injections over 2–4 d, yielding a progressive increase in the amount of antibody administered. Patients are injected with individual doses while positioned in a gamma camera, and imaging is initiated at the start of the injection. The acquisition is performed in dynamic mode with images collected at several time intervals over 1 h. Using software developed in-house, images are corrected for patient movement through iterative alignments, decay corrected, and summed to yield a series of images over regular time intervals. Parametric rate images are obtained by fitting a linear expression to the counts in each pixel. In this study, rate images from a patient's first injection were compared with rate images from the last injection. **Results:** The conventional planar images of antibody distribution showed significant uptake in liver, spleen, and marrow, whereas the generated rate images displayed different patterns, sometimes with negative values in liver and spleen and positive values in marrow, reflecting clearance and uptake rates rather than total accumulation. The impact of the progressive increase in antibody administration was observed by comparing the first with the last rate images. Interpatient comparisons were also made and showed that rate image patterns varied depending on patient-specific conditions such as the amount of disease and previous therapies undergone by the patient. **Conclusion:** Rate images make it possible to succinctly display kinetic information about an agent's behavior over the entire acquired image.

**Key Words:** parametric imaging; pharmacokinetics; radiolabeled antibodies; Bi213-HuM195; clearance rates

**J Nucl Med 2001; 42:27–32**

---

**W**hen radiolabeled antibody images are part of a temporal series, pharmacokinetic analysis can provide a map of the behavior of an agent. Typically, kinetic data are obtained by the delineation of preselected organs or regions of interest, which are then converted to counts per region and fit to a function for further analysis (1). Because this method depends on drawing by individual users and an a priori assumption concerning the areas of changing uptake and clearance, it is possible to truncate or miss entirely areas that may be of interest in terms of an agent's kinetic activity.

As an alternative to user selection and drawing of regions, we have developed an approach that examines the entire acquired image and generates a pixel-by-pixel representation of parametric values (2–4). The image alignment, decay correction, and other tools necessary for the successful generation and comparison of whole-body parametric images have been incorporated into an in-house software package, Multiple Image Analysis Utility (MIAU) (5,6).

To illustrate the method, we generated parametric images for selected patients enrolled in a phase I trial using Bi213-HuM195 for the treatment of myeloid leukemia (7–9). HuM195 is a humanized monoclonal antibody reactive with the early myeloid surface antigen, CD33 (10). The requirements of the Bi213 protocol include multiple injections wherein all patients were imaged after the first and last injections. Using these data, we were able to make comparisons between images generated from the first and last imaging sessions as well as across different patients.

## MATERIALS AND METHODS

Four patients with varying levels of disease, as measured by peripheral cell counts and bone marrow biopsy, and varying levels of response to the Bi213-HuM195 therapy were selected for illustration of the technique (Table 1). Total activity was administered in four to eight separate injections over a 48-h period with antibody amounts ranging from 0.53 to 1.63 mg. Because Bi213 has a short half-life (45.6 min), patients were injected while positioned under a dual-head gamma camera, and a series of simultaneous anterior and posterior images were acquired in dynamic mode (8). Images were collected over 1 h in two groups consisting of thirty 1-min frames and then ten 3-min frames for a total of 40 images. Because imaging is started at the same time as the antibody is

---

Received Dec. 17, 1999; revision accepted Jul. 6, 2000.

For correspondence or reprints contact: Katherine S. Kolbert, MS, Department of Medical Physics, Memorial Sloan-Kettering Cancer Center, 1275 York Ave., New York, NY 10021.

**TABLE 1**  
Administered Antibody and Disease Assessment per Patient

Patient no.	Antibody dose (mg)			Bone marrow blasts (%)		WBCs*	
	First	Last	Total	Before treatment	After treatment	Before treatment	Nadir
1	1.630	1.480	4.590	38	24	2.8	0.1
2	0.699	0.653	5.071	28	6	1.8	0.4
3	0.898	0.891	3.585	67	50	3.2	0.9
4	1.18	1.03	3.37	20	11	5.6	0.2

\* WBCs = white blood cells in thousands of cells/mm<sup>3</sup>.

injected, antibody uptake curves for these patients showed an initial period of rapid uptake corresponding to the period of rapid antibody infusion followed by a plateau (8). Therefore, for the purpose of generating parametric images, the first six 1-min images, corresponding to injection and clearance from the injection site, were eliminated from the dynamic series. The remaining 34 images from each treatment imaging session were read into MIAU for further processing.

The first step was to separate the biologic behavior of the antibody from the effect of isotope physical decay by decay correcting each pixel value within each image of an acquisition series to time = 0, the time of injection. The pixel values were also smoothed using a boxcar averaging technique of width 5 to cut down on subpixel misalignment and to reduce artifacts associated with the low counting statistics of individual pixels. Spatial correspondence between the individual images in a series was established using the first image as reference and aligning the remaining images in the series to it using the manual translation or rotation and region-of-interest tools in MIAU (5,6).

To have each image within an acquisition series represent a uniform time period, the 1-min images acquired during the first 30 min were combined by image addition so that each of the resulting five images represented equal 6-min time periods. The 3-min images from the second half of each imaging series were then added in groups of two, resulting in four additional 6-min images for a total of nine images.

The counts of spatially corresponding pixels from each of the combined images within a treatment were fit to a linear expression of counts versus time, and the calculated slope was inserted into a two-dimensional matrix (Fig. 1), referred to here as a rate or parametric image. A linear expression was chosen on the basis of the conventional analysis of liver, spleen, and red marrow kinetics in the phase I study (8). By examining the magnitude of the slope, it is possible to determine the rate at which the agent is clearing or accumulating at that point by considering a positive slope to represent uptake and a negative slope to represent clearance. Using the color scale that we selected for the rate image, when the slope of the line passing through the points is positive, the rate of accumulation (in counts per minute [cpm]) is increasing and the color is in the red-orange range. Conversely, when the slope is negative, the rate of change is decreasing and the color is in the blue-green range. All parametric images are displayed using this color scale showing the full range of changing rate values for that image set in counts per minute. When there is no change in the rate of accumulation or clearance of the agent, the slope is flat or zero and the corresponding image color is indicated on the color scale by 0.0.

Parametric images were generated using the anterior and posterior sets of planar dynamic images and scaled to the same maximum and minimum rate of change within each patient for comparative purposes. To further enhance a visual comparison between patients, the same minimum and maximum values were used across the entire group of patients whenever possible.

Images were displayed showing the anterior and posterior views of each patient for the first and last injections side by side. To compare these images with conventional images and to establish a correspondence to the patient's anatomy, images from the dynamically acquired spot anterior and posterior views were summed and displayed below the parametric images. Isorate contours were generated from the parametric images to highlight regions showing varying rates of uptake or clearance and then were overlaid on the summed spot images.

## RESULTS

The parametric images generated for the four patients showed accumulation and clearance rates ranging from -0.3 to >4.0 cpm. To preserve small visual changes in rate that were lost when the same maximum and minimum values were used across all four patients, the parametric images were divided into two sets: images with rates between -4.0 and 5.0 cpm (patients 1 and 4) and between -1.0 and 1.0 cpm (patients 2 and 3).

Parametric images generated for patient 1 are shown in the top row of Figure 2. The calculated slope values range from -3.9 to 4.9 cpm as indicated by the rate scale. The anterior and posterior views of the rate image show a significant rate of clearance in the regions of the liver and spleen, whereas the region corresponding to the marrow shows varying rates of uptake. Isorate contours superimposed on the conventional, summed images in the bottom row confirm the anatomic location of these regions.

Parametric and conventional summed spot images of the second patient in the series are shown in Figure 3. Because the range of slope values for these images was between -0.7 and 0.9, the rate scale used is -1.0 to 1.0 cpm. In these images, regions corresponding to the liver, spleen, and marrow in the first injection show positive rates of uptake in the posterior view. However, the rate of uptake decreases between the first and last injections.

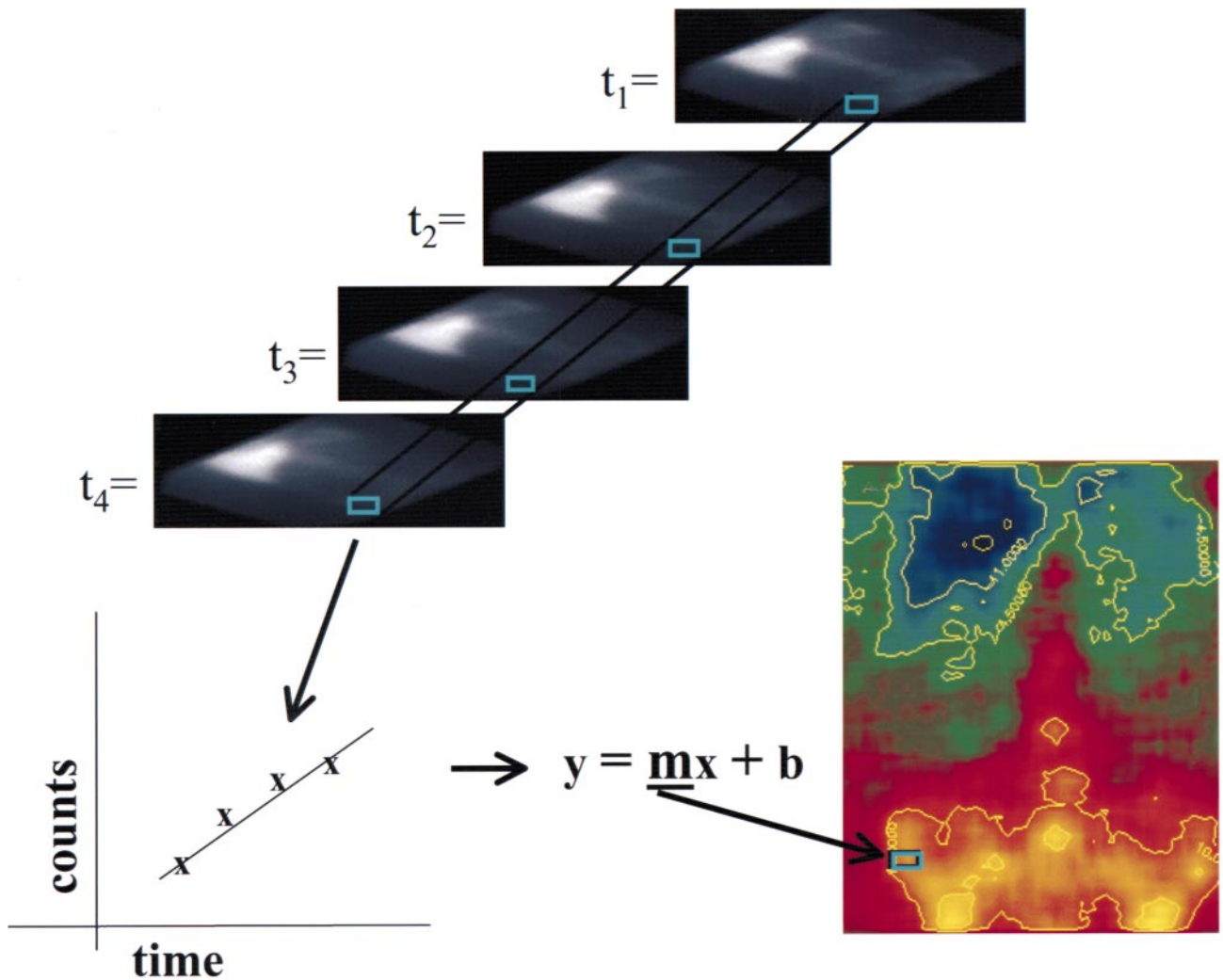


**FIGURE 1.** Pictograph of steps for generating parametric images. On top is series of four spot images taken at sequential time points. Spatially identical pixel (in green) has been selected from each image and fit to a line. Slope ( $m$ ) is placed in image matrix at corresponding point.

Parametric images generated for the third patient are shown in Figure 4 and are displayed using the same scale as for patient 2. It is more difficult to identify regions corresponding to specific organs on these images, and the rates of uptake and clearance are over a very narrow range, indicating no significant change in rate between the first and last injections.

Potential artifacts resulting from organ overlap and residual uncorrected organ or patient movement may arise when generating parametric images and must be considered. For instance, if the rate of uptake and the rate of clearance in two overlapping organs are the same, they will negate each other and show a flat rate of uptake or clearance, resulting in the appearance of a gap between the overlapping regions.

Movement, either by an individual organ or by the patient during the acquisition, results in small regions with very

high rate gradients. This is caused by the rapid changes in counts as the activity moves away and back under the camera.

Figure 5 illustrates artifacts associated with both patient and organ movement. The patient depicted has uptake and clearance rates that are similar to those of the first patient. In the region of the spleen on the posterior image from the first injection, there appears to be an area with a high rate of uptake adjacent to an area with a high rate of clearance. Separating these two regions is an area of flat rate change. Examination of the corresponding regions on the 60-min summation image indicates that these areas correspond to the edges of the spleen rather than to the spleen itself. In addition to an examination of the hip or pelvic region, these observations suggest that the characteristic pattern of an artifact caused by organ or patient movement is what is seen here.



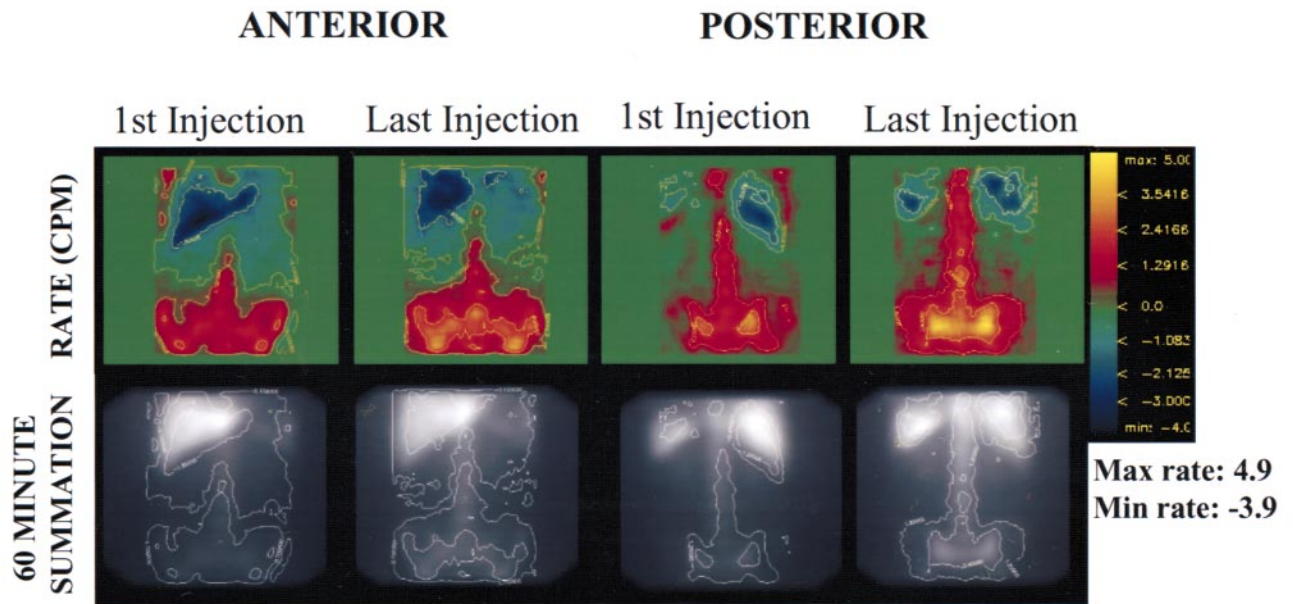


**FIGURE 2.** Top row shows parametric images of patient 1. Generated isorate contours of 0.7 and  $-1.8$  cpm are displayed on anterior view and 1.2 and 2.4 cpm are shown on posterior view. Isolevels are also superimposed on corresponding summed planar images in bottom row.

Image noise is another issue because the dynamically acquired images suffer from a low signal-to-noise ratio as well as low pixel counts. This contributes to the uncertainty of the rate estimate and is only partially compensated by smoothing of the image.

**DISCUSSION**

As opposed to images of total uptake over time, rate images provide kinetic information that may be used di-

rectly in mathematical modeling (e.g., to assess antigen density, which can be related to tumor burden (11) and antibody availability). By comparing interpatient and inpatient images, it may be possible to characterize differences in fitted parameters. Although the method is illustrated using dynamic data, the basic implementation is applicable to static data collected over longer time periods.

Patient 1 (Fig. 2) had extensive disease and showed the largest reduction in peripheral blood cells in response to

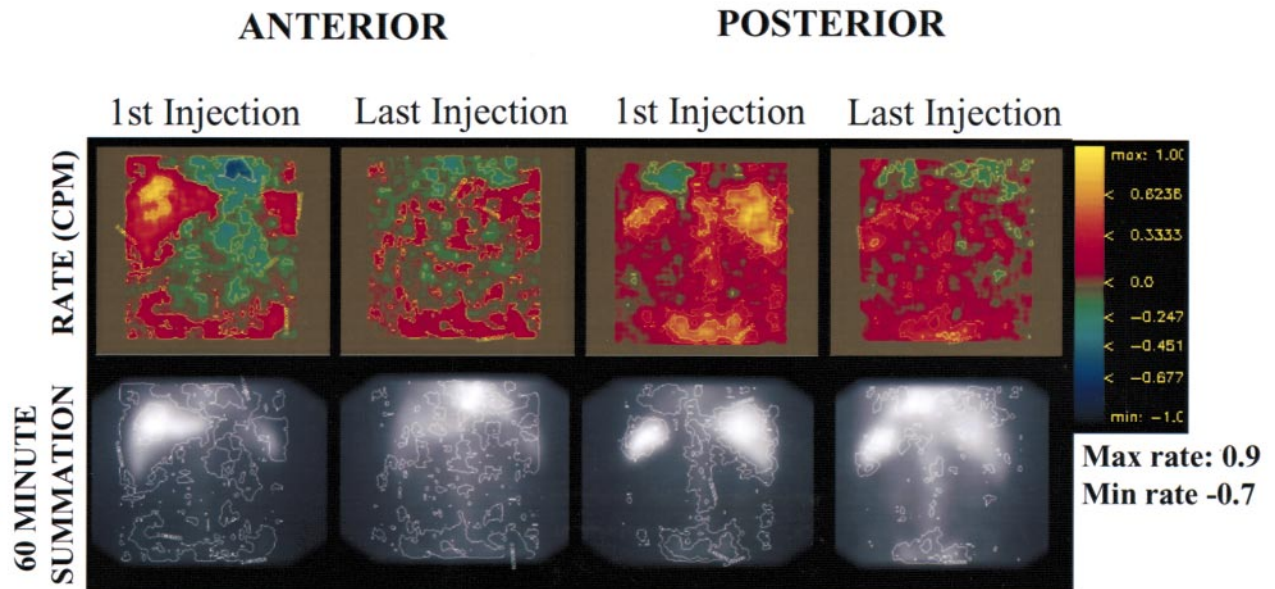


**FIGURE 3.** Anterior and posterior parametric images of patient 2 with isorate contours of  $-0.15$  and 0.08 cpm shown on anterior view and 0.25 and 0.45 cpm shown on posterior view.

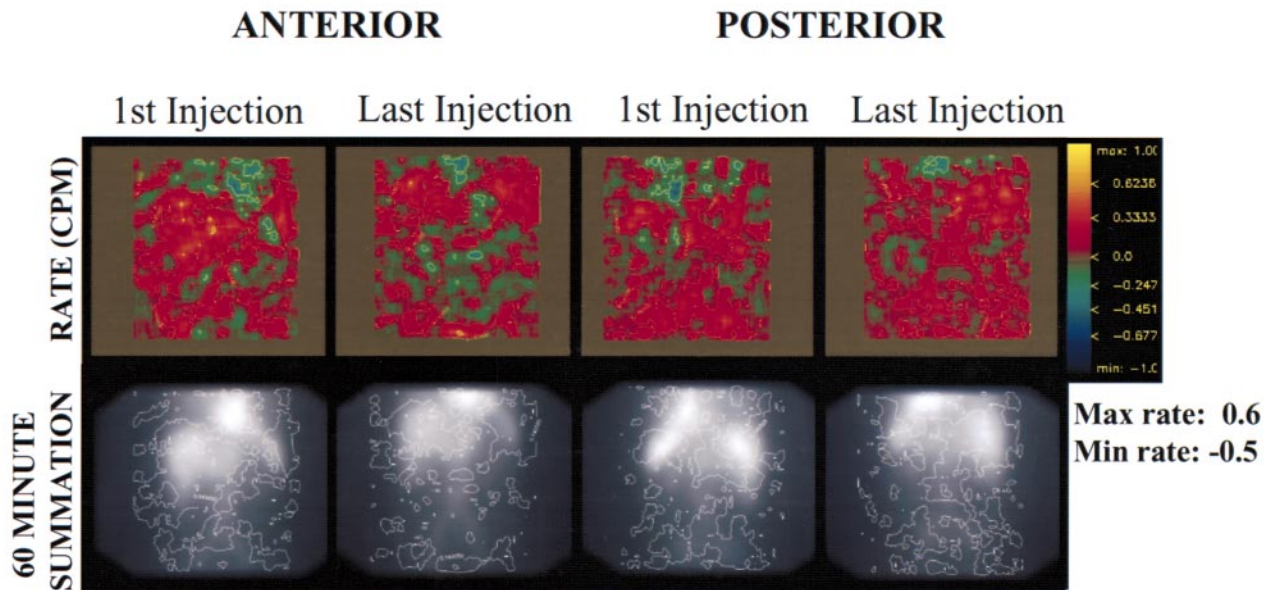


FIGURE 4. Parametric images of patient 3 show single isorate level of 0.14 cpm.

therapy in this group of selected patients, as indicated by comparing the white blood cell counts before therapy with the white blood cells at nadir (Table 1). It has been established that initial injections of Bi213-HuM195 are more likely to target easily accessible peripheral antigen sites (12–14). By the time of the last injection, these sites have been saturated, leaving the antibody to target sites in the marrow. On the parametric image of the first injection, the rate of uptake in the region of the spine and pelvis is clearly defined and is high relative to that of the other patients in the

series. In addition, comparing the rate image of the first injection with the last, it is clear that in the last injection the antibody is reaching and targeting antigen sites in the marrow at a greater rate, as seen by the higher pixel intensities.

Comparing patient 2 (Fig. 3) with the previous one, the clinical data (Table 1) show that this patient also had a response to the therapy. However, relative to the previous patient, patient 2 had less initial disease, as indicated by a lower percentage of bone marrow blasts. On this patient's parametric images, a positive rate of uptake is

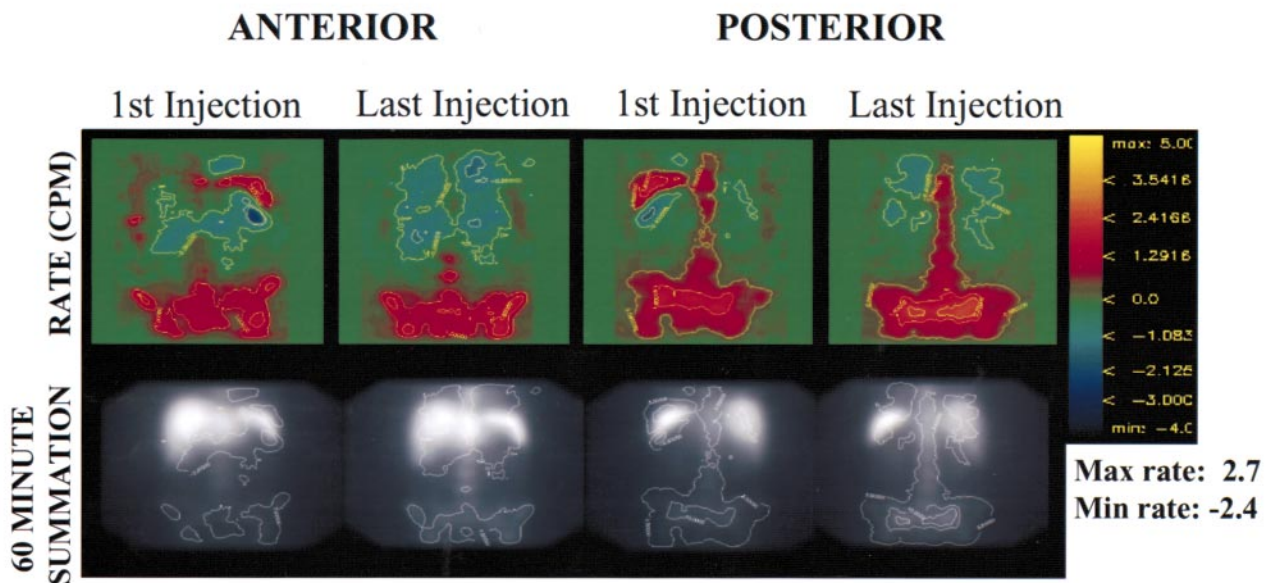


FIGURE 5. Parametric images of patient 4 show functional image artifacts. Movement that is apparent from rate image—particularly in hip and spleen region of posterior, first injection—cannot be plainly seen on conventional images.

visible in the posterior view. Comparing the last injection with the first, the rate of uptake is less in all regions. In this case, a possible interpretation of the rate images is that the initial injections were sufficient to target the peripheral sites and the sites in the marrow so that by the last injection these sites were saturated and the uptake rate was reduced.

The third patient (Fig. 4) is more complicated clinically than the previous two. This patient was given significant doses of unlabeled antibody in another study before entering this protocol. Although this patient did not have a detectable immune response after the previous exposure to HuM195, a low-level human antihuman response could have prevented the targeting of leukemia cells, thereby accounting for the lack of marrow uptake on these scans.

Although the parametric images of patient 4 show movement artifacts, it is still possible to notice that the range of accumulation rate and the pattern of greater intensity in the last rate image compared with first rate image are similar to those of the first patient. From the data shown in Table 1, patient 4 and patient 1 had the greatest reduction in white blood count at nadir of this group.

## CONCLUSION

We have developed a method for extracting kinetic data from standard gamma camera images that has been defined into a number of easily executed steps using software developed in-house. The parametric images of aggregate slope provide a visualization of the linear gradient of corresponding image pixels across the time series of dynamically acquired images and represent maps of the kinetic behavior of the agent in the body. This approach makes it possible to visually assess pharmacokinetics over an entire image without drawing regions of interest. The degree to which such information may impact patient management will be explored in ongoing implementations of this approach.

## ACKNOWLEDGMENTS

We thank Dr. Joseph O'Donoghue for his excellent insights concerning this work. Clinical grade  $^{225}\text{Ac}$  for the  $^{213}\text{Bi}$  gen-

erator was provided by PharmActinium, Inc. (Chevy Chase, MD); the European Institute for Transuranium Elements (Karlsruhe University, Karlsruhe, Germany); and the Department of Energy, Isotopes Production and Distribution. This research was supported by National Institutes of Health grants RO1CA62444, PO1CA33049, and RO1CA55349 and by Department of Energy grant DE-FG02-86ER-60407. This paper was presented, in part, at the Annual Meeting of the Society of Nuclear Medicine, Los Angeles, CA, June 6-10, 1999.

## REFERENCES

1. Watson EE, Stabin MG, Siegel JA. MIRD formulation. *Med Phys.* 1993;20:511-514.
2. Chen QS, Sgouros G, Zhang JJ, et al. Automated registration of planar images for improved diagnosis, region-of-interest analysis, and dosimetry [abstract]. *J Nucl Med.* 1995;36(suppl):86P.
3. Chen Q. Parametric imaging of patient pharmacokinetics. *Eur J Nucl Med.* 1997;24:1369-1373.
4. Kolbert KS, Jurcic JC, Larson SM, Scheinberg DA, Sgouros G. Parametric images of pharmacokinetics: clinical implementation in Bi-213-HuM195 therapy of leukemia [abstract]. *J Nucl Med.* 1999;40(suppl):41P.
5. Kolbert KS, Sgouros G. Display and manipulation of multi-modality images for radiolabeled antibody therapy. *Radiology.* 1998;209(suppl):515.
6. Kolbert KS, Sgouros G. Display and manipulation of SPECT and CT studies for radiolabeled antibody therapy [abstract]. *Cancer Bioth Radiopharm.* 1998;13:302.
7. Jurcic JG, McDevitt MR, Sgouros G, et al. Phase I trial of targeted alpha-particle therapy for myeloid leukemias with bismuth-213-HuM195 (anti-CD33) [abstract]. *Proc Am Soc Clin Oncol.* 1999;18:7a.
8. Sgouros G, Ballangrud AM, Jurcic JG, et al. Pharmacokinetics and dosimetry of an  $\alpha$ -particle emitter labeled antibody:  $^{213}\text{Bi}$ -HuM195 (anti-CD33) in patients with leukemia. *J Nucl Med.* 1999;40:1935-1946.
9. Nikula TK, McDevitt MR, Finn RD, et al. Alpha-emitting bismuth cyclohexylbenzyl DTPA constructs of recombinant humanized anti-CD33 antibodies: pharmacokinetics, bioactivity, toxicity and chemistry. *J Nucl Med.* 1999;40:166-176.
10. Caron PC, Dumont L, Scheinberg DA. Supersaturating infusional humanized anti-CD33 monoclonal antibody HuM195 in myelogenous leukemia. *Clin Cancer Res.* 1998;4:1421-1428.
11. Sgouros GS, Graham MC, Divgi CR, Larson SM, Scheinberg DA. Modeling and dosimetry of monoclonal antibody M195 (anti-CD33) in acute myelogenous leukemia. *J Nucl Med.* 1993;34:422-430.
12. Caron PC, Jurcic JG, Scott AM, et al. A phase 1B trial of humanized monoclonal antibody M195 (anti-CD33) in myeloid leukemia: specific targeting without immunogenicity. *Blood.* 1994;83:1760-1768.
13. Scheinberg DA, Lovett D, Divgi CR, et al. A phase I trial of monoclonal antibody M195 in acute myelogenous leukemia: specific bone marrow targeting and internalization of radionuclide. *J Clin Oncol.* 1991;9:478-490.
14. Schwartz MA, Lovett DR, Redner A, et al. Leukemia cyto-reduction and marrow ablation after therapy with  $^{131}\text{I}$  labeled monoclonal antibody M195 for acute myelogenous leukemia (AML). *J Clin Oncol.* 1993;11:294-303.